Direct Photochemical Patterning and Refunctionalization of Supported Phospholipid Bilayers

Chanel K. Yee, Meri L. Amweg, and Atul N. Parikh*

Contribution from the Department of Applied Science, University of California, Davis, California 95616

Received April 20, 2004; E-mail: anparikh@ucdavis.edu

Abstract: A wet photolithographic route for micropatterning fluid phospholipid bilayers is demonstrated in which spatially directed illumination by short-wavelength ultraviolet radiation results in highly localized photochemical degradation of the exposed lipids. Using this method, we can directly engineer patterns of hydrophilic voids within a fluid membrane as well as isolated membrane corrals over large substrate areas. We show that the lipid-free regions can be refilled by the same or other lipids and lipid mixtures which establish contiguity with the existing membrane, thereby providing a synthetic means for manipulating membrane compositions, engineering metastable membrane microdomains, probing 2D lipid—lipid mixing, and designing membrane-embedded arrays of soluble proteins. Following this route, new constructs can be envisaged for high-throughput membrane proteomic, biosensor array, and spatially directed, aqueous-phase material synthesis.

Introduction

Supported phospholipid bilayer membranes (sBLMs) have been a subject of great attention because of their extraordinary ability to preserve many biophysical properties of cellular membranes.[1] Sustained interest in these materials can be attributed to two factors. First, they are proving to be useful material constructs for modeling many reaction—diffusion processes that characterize structure, assembly, dynamics, and functions of complex, heterogeneous biological membranes.[2] Key applications include phase stability and dynamics (e.g., membrane polymorphism,[3] lipid—lipid phase separation,[4] lipid rafts,[5] and complex diffusion[6]), protein—membrane interactions (receptor clustering and colocalization,[7] pattern formation,[8,9] and pore formation[10]), ligand—receptor interactions within single membranes, and membrane—membrane processes such as fusion[11] and adhesion.[12] These processes are relevant to broad classes of biological mechanisms, e.g., cellular signaling,[13] vesicle trafficking, immune response,[14] programmed cell death or apoptosis,[15] cell adhesion[16] and fusion,[17] and host—pathogen

interactions.[18] Second, since supported membranes integrate fluid phospholipid structure with a solid surface, they are relevant in the design of synthetic biocompatible surfaces[19] and many membrane-based biosensing[20,21] and drug-discovery platforms.[22]

Structurally, supported membranes represent a class of bimolecular interfacial films composed essentially of two apposing monolayers of phospholipids.[23] They are typically formed at the solid—liquid interface when vesicular microphases of lipids and their mixtures rupture and spread spontaneously on hydrophilic surfaces,[24,25] but two successive transfers of lipidic monolayers from the air—water interface onto planar surfaces in Langmuir—Blodgett schemes have also been used.[26] When appropriately formed, they are essentially separated from the substrate surface through an intervening cushion layer[27,28] (e.g., a hydration layer of water $10-15$ Å thick on silica surfaces) and exhibit two-dimensional contiguity and fluidity reminiscent of lipid membranes of vesicles and living cells.[2,29]

(1) Sackmann, E. *Science* **1996**, *271*, 43−48.
(2) Boxer, S. G. *Curr. Opin. Chem. Biol.* **2000**, *4* 704−709.
(3) Welti, R.; Glasser, M. *Chem Phys. Lipids* **1994**, *73*, 121−137.
(4) Wolf, D. E. *Curr. Top. Membr.* **1994**, *40*, 143−165.
(5) London, E. *Curr. Opin. Struct. Biol.* **2002**, *12*, 480−486.
(6) Ratto, T. V.; Longo, M. L. *Biophys. J.* **2002**, *83*, 3380−3392
(7) Orth, R. N.; Wu, M.; Holowka, D. A.; Craighead, H. G.; Baird, B. A. *Langmuir* **2003**, *19*, 1599−1605.
(8) Heyse, S.; Stora, T.; Schmid, J. H.; Lakey, J. H.; Vogel, H. *Biochim. Biophys. Acta* **1998**, *137*, 319−338.
(9) Damjanovich, S.; Gaspar, R.; Pieri, C. *Q. Rev. Biophys.* **1997**, *30*, 67−106.
(10) Zuckermann, M. J.; Heimburg, T. *Biophys. J.* **2001**, *81*, 2458−2472.
(11) Tamm, L. K.; Crane, J.; Kiessling, V. *Curr. Opin. Struct. Biol.* **2003**, *13*, 453−466.
(12) Groves, J. T.; Dustin, M. L. *J. Immunol. Met.* **2003**, *278*, 19−32.
(13) Wulfing, C.; Sjaastad, M. D.; Davis, M. M. *Proc. Natl. Acad. Sci. U.S.A.* **1998**, *95*, 6302−6307.
(14) Dykstra, M.; Cherukuri, A.; Sohn, H. W.; Tzeng, S. J.; Pierce, S. K. *Annu. Rev. Immunol.* **2003**, *21*, 457−481.
(15) de Nigris, F.; et al. *Trends Mol. Med.* **2003**, *9*, 351−359.
(16) Takagi, J.; Springer, T. A. *Immunol. Rev.* **2002**, *186*, 141−163.
(17) Chernomordik, L. V.; Kozlov, M. M. *Annu. Rev. Biochem.* **2003**, *72*, 175−207.
(18) Kahn, R. A.; Fu, H.; Roy, C. R. *Trends Biochem. Sci.* **2002**, *27*, 308−314.
(19) Sackmann, E.; Tanaka, M. *Trends Biotechnol.* **2000**, *18*, 58−64.
(20) Bayley, H.; Cremer, P. S. *Nature* **2001** *413*, 226−230.
(21) Cornell, B. A.; BraachMaksvytis, V. L. B.; King, L. G.; Osman, P. D. J.; Raguse, B.; Wieczorek, L.; Pace R. J. *Nature* **1997**, *387*, 580−583.
(22) Groves, J. T. *Curr. Opin. Drug Discovery Res.* **2002**, *5*, 606−612.
(23) Tamm, L. K.; McConnell, H. M. *Biophys. J.* **1985**, *47*, 105−113.
(24) Keller, C. A.; Glasmastar, K.; Zhdanov, V. P.; Kasemo, B. *Phys. Rev. Lett.* **2000**, *84*, 5443−5446.
(25) Johnson, J. M.; Ha, T.; Chu, S.; Boxer, S. G. *Biophys. J.* **2002**, *83*, 3371−3379.
(26) Wenzl, P.; Fringeli, M.; Goette, J.; Fringelli, U. P. *Langmuir* **1994**, *10*, 4253−4264.
(27) Bayerl, T. M.; Bloom, M. *Biophys. J.* **1990** *58*, 357−362.
(28) Johnson, S. J.; et al. *Biophys. J.* **1991**, *59*, 289−294.
(29) McConnell, H. M.; Watts, T. H.; Weis, R. M.; Brian, A. A. *Biochim. Biophys. Acta* **1986**, *864*, 95−106.

Recently, there has been a great interest in spatially patterning supported membranes for localizing and parallelizing membrane functions.[30] In this regard, two critical requirements must be met. First, because phospholipid membranes are fluid supramolecular assemblies and their functions are closely associated with their microenvironment, a key to patterning membrane functions is the development of approaches that allow confining bilayer patches, rather than individual molecules, over the substrate surface within predefined substrate regions. The second requirement stems from the need to maintain the bilayers under aqueous conditions for preserving their biophysical fluidity and function. The patterning method, therefore, must be applicable under wet conditions.

Previously, micropatterning of sBLMs has been achieved by a variety of methods that conveniently fall into two broad categories.[31-39] First, several multistep, indirect methods have been reported that use prepatterned substrate surfaces which present physical, chemical, and/or electrostatic barriers to membrane formation[33] or allow a selective lift-off process.[7] Many of these methods circumvent the requirements of wet ambients by employing prepatterned surfaces. Typically, patterns of barrier materials are deposited onto substrate surfaces using controlled deposition techniques such as photolithography, e-beam lithography, and microcontact printing. Barrier materials have included metals and metal oxides,[33] photoresists,[40] proteins,[34] and even photopolymerizable lipids,[35,36] but simple mechanical scratches[32] have also proven useful. Second, soft lithography applications of poly(dimethylsiloxane) (PDMS) stamps for direct patterned deposition (stamping) or removal (blotting) have also proven successful.[38,39] But several limitations persist. The methods requiring substrate prepatterning depend on the prior deposition of exogenous materials on the substrate surface and form single, permanent patterns. Moreover, the mechanisms by which barrier materials compartmentalize membrane patterns remain poorly understood. For instance, while aluminum oxide resisted vesicle spreading, deposition of lipids, albeit immobile, was noted for chrome, gold, and indium−tin oxide surfaces.[33] Methods based on PDMS stamps, on the other hand, require optimization of the contact time and associated contact pressure for different lipid compositions.[41] Further, an additional unresolved issue in creating patterned supported membranes using stamping is the possible reversal of leaflets in asymmetric bilayers which may result due to the transfer process.

Here, we describe a simple light-directed alternative for directly patterning microvoids or holes that serve as fluidity barriers within supported membranes. The method uses a spatially directed illumination of preformed supported phospholipid bilayers by short-wavelength ultraviolet radiation. The patterned exposure using a Hg source and a physical mask results in highly localized photodecomposition of the exposed lipids, leaving the unexposed lipids fluid. The method is applicable for patterning bilayers deposited on large substrates, does not require prior substrate modifications, and is independent of bilayer composition and compositional asymmetry. Using this method, we can directly engineer stable patterns of hydrophilic voids within a fluid membrane. Furthermore, the voids can be refilled by targeted rupture of secondary lipid vesicles which can establish contiguity with the existing membrane, thereby providing a synthetic means for probing 2D reaction−diffusion processes, manipulating membrane compositions, and creating functional microdomains in well-defined patterns. The approach broadly parallels solid-state lithographic methods developed for dry-state DNA and peptide arrays[42] but employs spatially defined photochemical degradation and is applicable for the aqueous-phase fluid bilayers.

Experimental Section

Materials. 1,2-Dimyristoyl-*sn*-glycero-3-phosphocholine (DMPC), 1-palmitoyl-2-oleoyl-*sn*-glycero-3-phosphocholine (POPC), and GM_1 ganglioside (brain, ovine ammonium salt) were obtained from Avanti Polar Lipids (Alabaster, AL). Texas Red-labeled 1,2-dihexadeconoyl-*sn*-glycero-3-phosphoethanolamine triethylammonium salt (TR-DHPE) and *N*-(7-nitrobenz-2-oxa-1,3-diazol-4-yl)-1,2-dihexadecanoyl-*sn*-glycero-3-phosphoethanolamine (NBD-DHPE) were obtained from Molecular Probes (Eugene, OR). All lipids were suspended and stored in chloroform or a chloroform/alcohol mixture in the freezer (−20 °C) until use. Cholesterol and sphingomyelin were purchased from Sigma-Aldrich (Milwaukee, WI), whereas hydrogen peroxide (30% v/v) and sulfuric acid were purchased from J. T. Baker (Phillipsburg, NJ) and Fisher Chemicals (Fairlawn, NJ), respectively, and used as received. All organic solvents were HPLC grade. All chemicals were used without further purification. Organic-free deionized water of high resistivity (approximately 18.0 mΩ cm) was obtained by processing water first through a reverse osmosis deionization unit and then a Milli-Q Plus water unit (model ZD40-11595, Bedford, MA) consisting of a five-bowl purification system (equipped with two Ion-Ex cartridges, one Super-C cartridge, one Organex-Q cartridge, and an additional ultra-filtration cartridge). Phosphate-buffered saline (PBS; pH 7.2; 154 mM NaCl, 1.54 mM KH_2PO_4, and 2.71 mM Na_2HPO_4) was obtained from Gibco- Life Technology (Rockville, MD) and used as a vesicle spreading solution and buffer medium. Corning glass coverslips (no. 11/2, 22 mm², Fisher HealthCare, Houston, TX) were used as substrates unless noted otherwise. Silicon substrates with native oxide overlayers (Silicon Sense, Nashua, NH) were also used in control experiments.

Formation of Supported Lipid Bilayers. Supported phospholipid bilayers were formed primarily using the previously reported vesicle fusion and rupture method.[33] Briefly, small unilamellar vesicles (SUVs) were prepared using vesicle extrusion methods.[43] Typically, a desired amount of lipid or lipid mixture suspended in chloroform or a chloroform/alcohol mixture was mixed in a glass vial. The solvent phase was then evaporated under a stream of nitrogen and subsequently evacuated for at least 1 h in a vacuum desiccator. The dried lipid mixture was then suspended in Millipore water and kept at 4 °C to be rehydrated overnight. The total lipid concentration was 2 mg/mL. The desired amount of hydrated aqueous solution was then sonicated and passed through an Avanti miniextruder (Avanti, Alabaster, AL) using 0.1 μm polycarbonate membrane filters (Avanti) 21 times at a desired tem-

(30) Groves, J. T.; Boxer, S. G. *Acc. Chem. Res.* **2002** *35*, 149−157.
(31) Groves, J. T.; Boxer, S. G. *Biophys. J.* **1995**, *69*, 1972−1975.
(32) Groves, J. T.; Ulman, N.; Boxer, S. G. *Science* **1997**, *275*, 651−653.
(33) Groves, J. T.; Ulman, N.; Cremer, P. S.; Boxer, S. G. *Langmuir* **1998**, *14*, 3347.
(34) Kung, L. A.; Kam, L.; Hovis, J. S.; Boxer, S. G. *Langmuir* **2000**, *16*, 6773−6776.
(35) Morigaki, K.; Baumgart, T.; Offenhausser, A.; Knoll W. *Angew Chem., Int. Ed.* **2001**, *40*, 172−174.
(36) Morigaki K.; Baumgart T.; Jonas U.; Offenhausser A.; Knoll W. *Langmuir* **2002**, *18*, 4082−4089.
(37) Cremer, P. S.; Yang, T. L. *J. Am. Chem. Soc.* **1999**, *121*, 8130−8131.
(38) Hovis, J. S.; Boxer, S. G. *Langmuir* **2000**, *16*, 894−897.
(39) Hovis, J. S.; Boxer, S. G. *Langmuir* **2001**, *17*, 3400−3405.
(40) Ulman, N.; Groves, J. T.; Boxer, S. G. *Adv. Mater.* **1997**, *9*, 1121−1123.
(41) Glasmastar, K.; Gold, J.; Andersson, A. S.; Sutherland, D. S.; Kasemo, B. *Langmuir* **2003**, *19*, 5475−5483.

(42) Fodor, S. P. A.; Read, J. L.; Pirrung, M. C.; Stryer, L.; Lu, A. T.; Solas, D. *Science* **1991**, *252*, 767.
(43) Mayer, L. D.; Hope, M. J.; Cullis, P. R. *Biochim. Biophys. Acta* **1986**, *858*, 161−168.
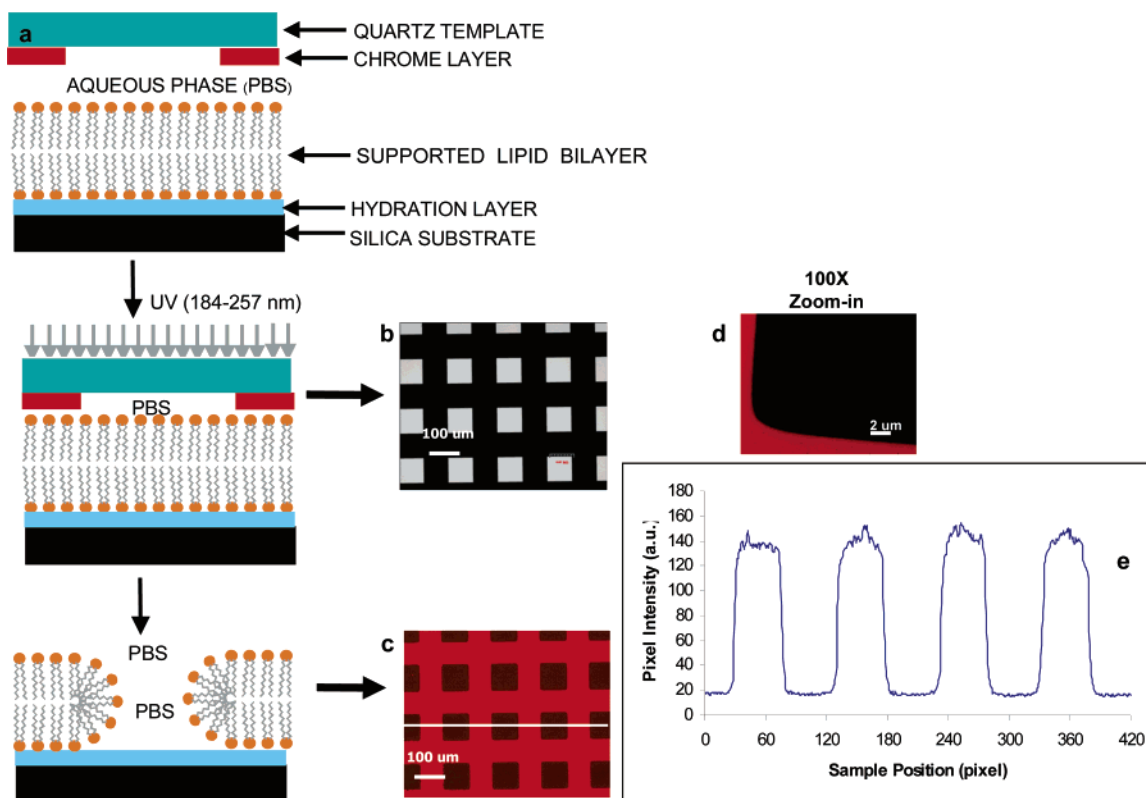
Figure 1. Direct patterning of void arrays within bilayer membranes using deep UV photolithography. (a) A schematic diagram of the key process steps. (b) Bright-field image of 100 μm square features on the quartz/chrome mask, where bright squares are quartz and dark regions reveal the chrome background. (c) Epifluorescence images of POPC bilayers containing 1 mol % TR-DHPE revealing resultant fluorescence patterns. (d) A high-magnification (100× (reproduced at 62% of original size), 1.4 NA) fluorescence image of the sharp boundary between the UV-exposed and UV-protected regions. (e) Fluorescence intensity profile across an arbitrarily chosen line spanning four alternating UV-exposed and unilluminated bilayer regions.

perature (typically 10 °C above the transition temperature for the major lipids). One part of the resulting SUV solutions was diluted with one part of PBS and stored at 4 °C until use. Typically, the SUV solutions were used within a day.

Substrates (silicon oxide wafers or Corning glass coverslips) pretreated for bilayer deposition were immersed in a freshly prepared 4:1 (v/v) mixture of sulfuric acid and hydrogen peroxide for a period of 4−5 min maintained at ∼100 °C. (*Caution: this mixture reacts violently with organic materials and must be handled with extreme care.*) The substrates were then withdrawn using Teflon tweezers, rinsed immediately with a copious amount of deionized water, and stored under water prior to use. Cleaned substrates were used within 1−2 h of the pretreatment. Bilayer samples were prepared by placing a clean substrate surface over a ∼80 μL SUV drop placed at the bottom of a crystallization well. The sample was allowed to incubate for approximately 5 min to ensure equilibrium coverage. The well was then filled with buffer solution and transferred to a large reservoir of buffer in which the substrate was shaken gently to remove excess vesicles. The supported bilayer samples prepared in this way were then stored in deionized water or PBS buffer for further use in UV lithography and characterization.

Selected samples were prepared following the vesicle spreading on phospholipid monolayers prepared by the Langmuir−Blodgett method.[23] Aliquots of 25−50 μL of a 1 mg/mL solution of DMPC in a 2:1 (v/v) chloroform/methanol mixture were spread drop-by-drop on the pure-water subphase surface of a constant-perimeter Langmuir trough (NIMA Technologies, England). The subphase pH was 5.6, and the temperature was monitored to be 21.2 ± 0.4 °C during the sample transfer. To ensure complete evaporation of the solvent phase, the subphase surface was left standing for at least 45 min. Monolayer transfers to solid substrates were carried out at a surface pressure of 30 mN/m at 25 mm/min. Only single monolayers were transferred during the upstroke

withdrawal of substrates from the subphase medium as judged by transfer ratios, which were found to be close to 100% within experimental error (±10%). The samples emerged visibly dry and were immediately used for vesicle spreading. Hybrid bilayer samples were prepared by first self-assembling octadecyltrichlorosilane from a 1 μL/mL solution in hexadecane following previously reported procedures.[44] Briefly, freshly cleaned glass slides were immersed in the self-assembly solution for 45 min. The samples were then withdrawn, rinsed in chloroform, and used for vesicle spreading as above.

UV Photolithography of Substrate-Supported Phospholipid Bilayers. Spatially directed deep UV illumination of supported bilayers was achieved using a physical mask and a deep UV grid lamp as illustrated in Figure 1a. The mask displaying patterns of chrome over a quartz substrate was obtained from Photoscience, Inc. (Torrance, CA). UV radiation was produced using a medium-pressure Hg-discharge grid lamp (UVP, Inc., Upland, CA) in a quartz envelope, and maintained in a closed chamber in a chemical hood. While still under buffer, the mask was gently lowered onto the bilayer samples placed in a crystallization dish filled with PBS. The sample system was then carefully placed in a UV/ozone-generating environment such that the coverslips were about 0.2−5 mm away from the light source depending on the illumination geometry. (*Caution: direct exposure to short-wavelength UV light (187 nm, 254 nm) must be avoided, and appropriate eyewear must be worn. Care must be taken in venting the ozone by operating grid lamps under chemical hoods. The breathing of ozone in high concentrations is dangerous. An ozone concentration in excess of 0.1 ppm can cause irritation.*) The exposure period was approximately 10−20 min unless noted otherwise. The amount of buffer (or water) on the sample surface was optimized to ensure that the samples remain submerged during the entire illumination process.

(44) Allara, D. L.; Parikh, A. N.; Rondelez, F. *Langmuir* **1995**, *11*, 2357−2360.

During the illumination process, the sample temperature was noted to slightly increase, typically to $3-5$ °C above room temperature. When the UV/ozone process took place in water (pH $7-8$), the pH was found to increase by approximately 0.5 pH unit upon 15 min of UV irradiation. Following the exposure, the samples were immersed in a large buffer bath, mask separated from the substrate surface, and stored in buffer (or water) for further characterization.

Epifluorescence Microscopy. A Nikon Eclipse TE2000-S inverted fluorescence microscope (Technical Instruments, Burlingame, CA) equipped with an ORCA-ER (model LB10-232, Hamamatsu Corp., Bridgewater, NJ) or Retige-1300 CCD camera (Technical Instruments) and a Hg lamp as the light source was used to visualize all fluorescent samples. Two filter wheels, one containing a set of excitation filters and the other emission filters, were mounted in front of the light source and the CCD camera, respectively. An extra triple-band emitter was installed in the dichroic mirror cube for aiding in focusing through the eyepiece. Typically, images were taken using either a Plan Fluor 10× (NA, 0.25) or a Plan Fluor, ELWD, 20× (NA 0.45) objective (Nikon, Japan). High-resolution images were obtained using 100× (NA 1.4) oil-immersion objectives. Images were stored and processed using a simple PCI software (Compix, Inc., Cranberry Township, PA) augmented with a quantitative dynamic intensity analysis module. Fluorescence images taken with the Texas Red filter set were assigned the color red, and the images acquired with the FITC filters were assigned the color green. Excitation and emission maxima for the probes used were 583/601 nm for TR-DHPE and 463/536 for NBD-DHPE.

To characterize membrane fluidity, a simple method to assess fluorophore mobility within the membrane medium was employed. We used microscopy-based fluorescence photobleach recovery measurements by adapting the circular spot photobleaching method.[45] Here, a circular region of the fluorescent bilayer sample, $\sim 30-50$ μm in diameter, was illuminated at high power continuously at the excitation wavelength for the fluorophore through a Plan Fluor, ELWD, 60× (NA 0.70) objective for ~ 2 min. The exposure bleaches a dark spot on the bilayer caused by the photoexcitation of the fluorophore followed by an irreversible chemical transformation effected by its reaction with oxygen dissolved in the ambient buffer. After photobleaching, the illumination path was replaced by a low-power observation beam through a 10× objective to record wide-field images of fluorescence recovery in the bleached area at 10 s intervals. The subsequent lateral motion of unperturbed fluorophore lipids from the unbleached background into the bleached spot (and vice versa) is recorded in the recovery profiles. It has been previously established that the precise shape of the recovery curve can be used to qualitatively characterize the nature of the fluorophore motion.[45] Furthermore, for diffusion-like motions, the measurements of the time required for the fluorescence intensity to recover halfway ($t_{1/2}$) between its immediate postbleach value and its long-time asymptotic value was used to estimate the diffusion coefficient, D, a measure of the fluidity of the bilayer environment.[46,47] Specifically, we followed a method developed by Yguerabide and Foster[46] which approximates the solution of the two-dimensional lateral diffusion equation using a modified Bessel function. Here, the experimental fluorescence intensity vs time data are replotted as reduced intensity vs time. Here, the reduced intensity is given by $I(\text{red}) = [I(t) - I(\infty)]/[I(0) - I(\infty)]$, where $I(t)$, $I(0)$, and $I(\infty)$ correspond to the fluorescence intensity at time t upon photobleaching, the prebleaching fluorescence intensity, and the long-time asymptotic recovery fluorescence intensity, respectively. The plot is then used to estimate $t_{1/2}$, which is in turn used to calculate $D = 0.22R_0^2/t_{1/2}$, where R_0 refers to the initial size of the photobleached spot. Next, we plotted the reduced fluorescence intensity against normalized time ($=Dt/R_0^2$)

using the estimated D values to compare the shape of the experimental normalized recovery curve with that of the theoretical curve[46] to qualitatively assess if the experimental mobilities are diffusion-like. Finally, a comparison between the prebleach intensity and the asymptotic fluorescence intensity was used to assess the presence of any immobile fractions. Note that the exposure time (~ 120 s) required in objective-based photobleaching introduces some, bilayer-fluidity-dependent, inaccuracies in the measurements of exact diffusion constants for probe lipids.

Attenuated Total Reflection Fourier Transform Infrared (ATR-FTIR) Spectroscopy. ATR-FTIR spectra[48] were recorded using a Bruker Equinox 55 Fourier transform infrared spectrophotometer equipped with a horizontal ATR accessory (Spectra-Tech, Inc., Shelton, CT) and DTGS detector (Bruker, Göttingen, Germany). The mid-IR spectra in the frequency range of $4000-600$ cm^{-1} were obtained at a 2 cm^{-1} resolution for 400 scans using a Blackman Harris three-term apodization. The spectrometer was purged with dry and carbon dioxide-free air. Ge trapezoids (45°), mounted in a boat configuration to allow liquid ambients, were used as the internal reflection element (IRE). The number of active internal reflections in the IRE was $N = 12$. For a careful determination of peak positions, the interferrograms were zero-filled to increase the point density by a factor of 2. The data analysis was performed using Grams 32 (Galactic Industries, Salem, NH) software.

Before use, the IREs were cleaned by a brief exposure to UV radiation followed by extensive rinsing in Millipore water. A single POPC bilayer was deposited by covering the IRE element with freshly extruded vesicles in the spreading buffer solution for a period of $5-10$ min. The spreading solution was then exchanged with Millipore water by rinsing the IRE surface several times to remove the excess vesicles while ensuring that the surface was always buried under water. The bilayer-coated samples were subsequently exposed to UV radiation using low-pressure Hg pen-ray lamps (UVP, Inc.) encapsulated in a quartz tube for an extended duration (~ 90 min). The longer durations were necessary because of the larger lamp–sample distances required by our illumination conditions and lower power achieved using the pencil lamps in real-time measurements.

Results

Epifluorescence Measurements. Epifluorescence microsopy was used to visualize the fluorescence patterns formed by the masked UV exposure of bilayer samples supported on glass coverslips. An example of an epifluorescence emission image for POPC bilayers doped with 1 mol % TR-DHPE probes is shown in Figure 1c. The high-contrast fluorescent pattern is comprised of dark features, essentially devoid of fluorescence emission, separated by a bright and homogeneous fluorescent background. A comparison of the bright-field image of the photomask (Figure 1b) and the corresponding epifluorescence image of the patterned bilayer (Figure 1c) reveals that the sizes and shapes of the fluorescence patterns are generally comparable replicas of the mask pattern. The patterns in fluorescence images correspond directly to the patterns of illumination: the exposed region corresponding to quartz (UV-transparent) regions of the mask was dark, and the unexposed (UV-opaque) region associated with chrome patterns continued to exhibit fluorescence. Prior to UV exposure, the samples displayed uniform fluorescence comparable to that of the protected areas of the patterned samples, suggesting that patterning conditions did not noticeably alter the protected parts of the bilayers. A line scan of fluorescence intensity shown in Figure 1e further reveals that the fluorescence intensity in several UV-exposed regions is

(45) Axelrod, D.; Koppel, D. E.; Schlessinger, J.; Elson, E.; Webb, W. W. *Biophys. J.* **1976**, *6*, 1055–1069.

(46) Grell, E., Ed. *Molecular Biology Biochemistry and Biophysics*; Springer-Verlag: Berlin, Heidelberg, Germany, 1981; pp 228–232.

(47) Koppel, D. E.; Axelrod, D.; Schlessinger, J.; Elson, E. L.; Webb, W. W. *Biophys. J.* **1976**, *16*, 1315–1329.

(48) Tamm, L. K.; Tatulian, S. A. *Q. Rev. Biophys.* **1997**, *30*, 365–429.
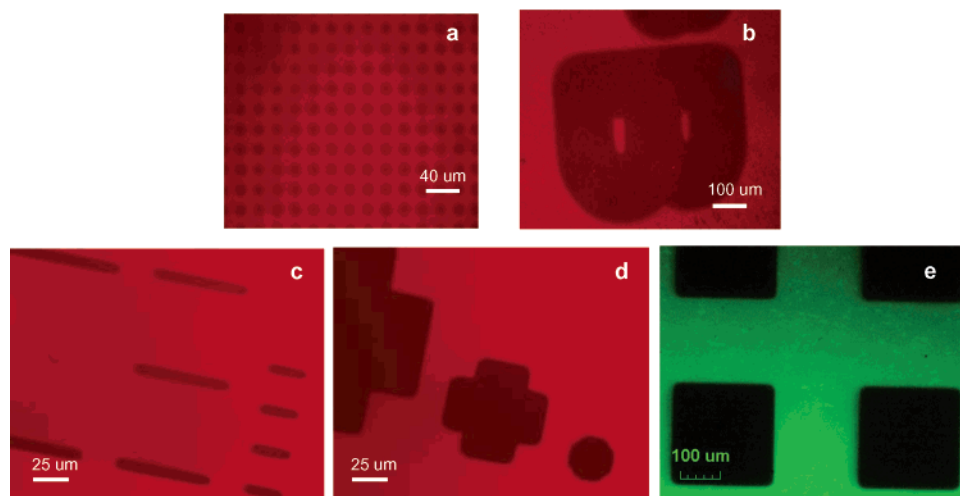
Figure 2. Epifluorescence images of UV-patterned TR-DHPE-doped egg-PC (a), POPC (b, c), and DMPC (d) bilayers showing various pattern sizes, shapes, and distributions. (e) An epifluorescence image of a UV-patterned lipid mixture bilayer (3% NBD-DHPE, 28% sphigomyelin, 10% cholesterol, 2% GM_1, and 57% POPC) on a hydrophilic glass substrate.

essentially constant, about the lowest value recorded. The finite value can be assigned to pixel "bleeding" peculiar to the CCD used in this study. Similarly, the scan also reveals that the fluorescence intensity in the unilluminated region is ~10-fold higher. We note that the actual contrast, taking into account the bleeding in our microscope configuration, is likely to be significantly larger.

A closer examination of the images using high-magnification objectives (100×, 1.4 NA, zoom-in of Figure 1d) shows that while sharp edges separate the fluorescent and dark regions, sharp corners of geometrical features on the mask always result in smoothly curved or rounded edges. This rounding-off was absent in the masks used. This observation can be attributed to the steric crowding and line-tension effects discussed later in the paper. We also note that occasionally the features showed enlargement or reduction in size probably due to slight off-parallel alignment between the mask and the sample surfaces that occasionally occurs in our illumination geometry. By deliberately applying the masks at angles with respect to the substrates, the feature amplification was controllably achieved. Note that the fluorescence patterns were visible directly after the UV exposure and no secondary development steps were necessary.

Examples presented in Figure 2 further elaborate the applicability of the approach for producing void patterns of arbitrary shapes, sizes, and densities at predetermined regions within the bilayer. Further, the approach was applicable for fabricating localized voids within contiguous bilayers as well as creating isolated membrane patches surrounded by lipid-free regions (Figure 2b). Using this approach, we were able to routinely produce feature sizes as small as 2 μm, separated by a 4 μm distance, covering the entire sample surface (e.g., a 22 × 22 mm^2 coverglass) and only limited by the size of the mask or the substrate itself. The limiting patternable sizes and densities have not yet been determined, but should be limited by a combination of the diffraction limit of the UV light, the attendant photochemical lipid oxidation, and any spreading of the residual bilayer at the edges (see the Discussion). Repeating the experiment using various fluorophores (e.g., Texas Red-, NBD-, and BODIPY-labeled DHPE lipid probes) and several phospholipids including DPPC, DPPE, DMPC, DLPC, POPC,

DOPC, and egg-PC and their mixtures (including sphingomyelin and cholesterol, Figure 2e) confirmed that the pattern formation using UV illumination was independent of the nature of the fluorophores, the phase state of the lipid, and chain unsaturation or the chemical character of the headgroup of the lipids used. Moreover, comparable results were obtained when bilayer preparation employed Langmuir–Blodgett and vesicle fusion methods. For a given lamp, we noted that the edge sharpness and definition of the patterns depended on several experimental parameters. We noted that several factors influenced the quality of the membrane fluorescence patterns. These include the (1) distance between the lamp and the sample, (2) distance between the mask and the sample, (3) ambient buffer pH and ionic strength, (4) exposure time, and (5) lamp cleanliness and power. Reproducibly sharp patterns in fluorescence resulted when the sample and mask were placed in a direct, soft contact submerged in PBS with a distance of ~0.2 mm from the lamp and a corresponding exposure period of 15 min in our illumination geometry.

The stability of the patterned features was assessed by observing the samples stored under water or aqueous buffer for several days. Daily examination of the patterns over a period of a week revealed the expected diminution of fluorescence intensity, whereas the sizes, shapes, and relative positions with respect to the substrate and among the features remained intact, indicating a long-term stability of the patterns. Bubbling nitrogen through the aqueous medium was observed to further improve the sample stability, presumably by reducing the rates of lipid oxidation. A preliminary thermal annealing experiment was found to alter the membrane fluorescence patterns. When patterned POPC bilayer samples (100 μm features) doped with 1 mol % TR-DHPE were heated to 65 °C, held for 30 min at 65 °C, and returned to room temperature, the fluorescence patterns showed evolution from well-defined patterns to those displaying ragged edges, ultimately leading to uniform lowered fluorophore intensity across the sample with no fluorescence trace of the pattern. These initial data suggest that the photochemical patterning process can be reversed by thermal annealing.

Imaging Fluorescence Photobleach Recovery. A simple adaptation of the widely used fluorescence photobleach recovery
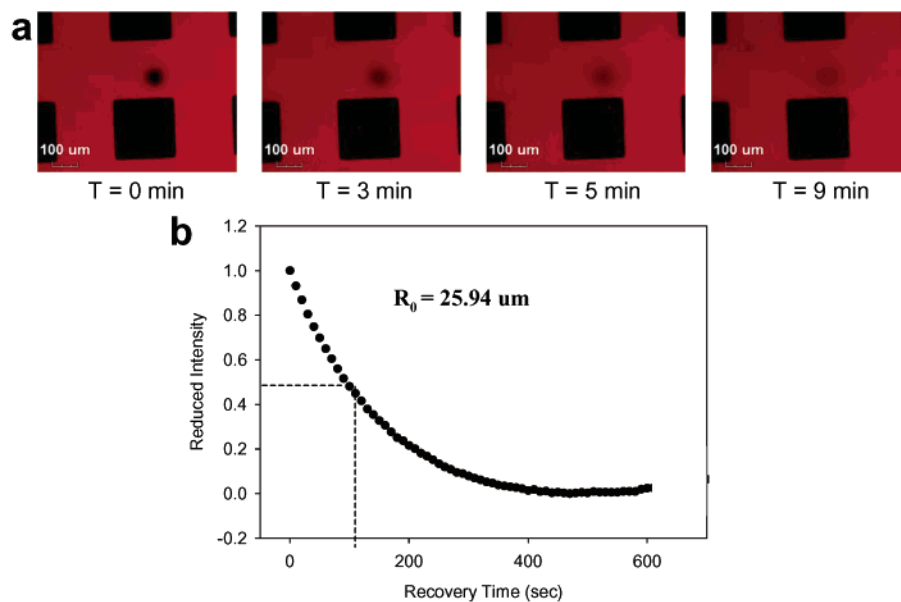
Figure 3. (a) Time-lapse epifluorescence images revealing the fluorescence recovery of an approximately 25 μm photobleached spot in a UV-protected region of a patterned POPC bilayer. The bilayer was doped with 1% TR-DHPE (see the text for details). (b) Fluorescence photobleach recovery curve normalized as reduced intensity (see the text) vs recovery time. $t = 0$ represents the time immediately after photobleach was determined complete. R_0 indicates the size of the bleached spot.

method was used to obtain a general assessment of the fluidity of phospholipid bilayers before and after UV patterning. Selected frames ($t = 0$, 3, 5, and 9 min) from a time-lapse sequence of images obtained during microscopy-based fluorescence photobleach recovery measurements for a UV-patterned POPC bilayer containing approximately 1 mol % TR-DHPE probe are shown in Figure 3a. Immediately following the photobleaching, a relatively sharp circular feature indicative of bleached fluorophores is seen. As a function of time, the fluorescence intensity within the spot is observed to gradually recover, ultimately leading to a uniform, lowered intensity across the image window. This behavior is qualitatively indicative of the translational mobility of the fluorophore within the contiguous parts of the bilayer structure. These data provide a strong confirmation that the intact bilayer in the protected part is two-dimensionally fluid. Such fluidity of the bilayer was observed to persist uniformly in all areas of the residual bilayer including in the close proximity of the pattern features.

An example of a typical normalized fluorescence recovery profile and the characteristic recovery time for a patterned POPC bilayer is also shown in Figure 3b. Following an approximation derived by Yuegbride and Foster,[45] we estimate the probe diffusion coefficient, D, to be ~1.8 ± 0.5 μm^2/s by averaging D over four different positions on the sample surface. Moreover, the shape of the recovery curve is consistent with a predominantly diffusion-like motion of the fluorophores.[45] Our estimates for the probe diffusion constant compare well with the average diffusion rate of ~2.0 ± 0.4 μm^2/s measured prior to UV exposure (data not shown). Further, these values are well within the range of 0.5–5 μm^2/s reported for fluid bilayers in previous studies.[49] In our measurements, there was no measurable disparity between the prebleach and long-time asymptotic fluorescence intensities, further suggesting the absence of any measurable amount of immobile lipid fractions for POPC bilayers. Taken together, these estimates suggest that the lipid
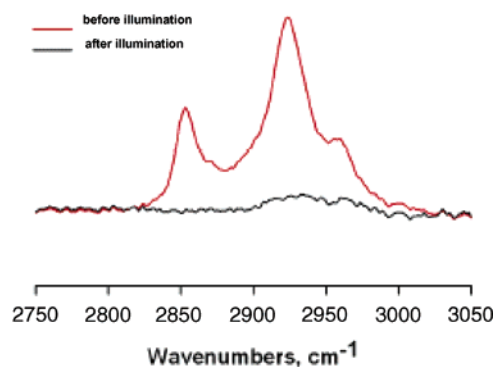

Figure 4. ATR-FTIR spectra in the acyl chain vibrational mode region (2750–3050 cm^{-1}) for an as-prepared POPC bilayer (red trace) and upon exposure to short-wavelength UV for 90 min (black trace).

bilayer in the UV-protected areas retains its overall fluidity. We note that the objective-based illumination for fluorescence recovery measurements used here is at best semiquantitative and did not allow precise determination of fluorophore diffusion coefficients. This was because relatively long exposure periods were required for photobleaching. Molecular motions of fluorophores during the photobleach period may lead to some unaccounted inhomogeneities in the fluorescence intensities.

Fourier Transform Infrared Spectroscopy. ATR-FTIR spectroscopy was used to obtain chemical characterization of the effects of UV illumination on the lipid molecules comprising the bilayer.

The solid trace (red) in Figure 4 represents the spectrum obtained for the as-prepared samples and the other trace (black) for the sample that had been exposed to UV radiation for an extended duration (~90 min). The spectrum for the unilluminated bilayer shows overlapping peaks with peak maxima at 2852, 2923, and 2964 cm^{-1} in the 2800–3000 cm^{-1} region. These peaks can be straightforwardly assigned to the methylene and methyl C–H stretching mode absorptions.[50] The details of

(49) Lee, G. M.; Jacobson, K. *Curr. Top. Membr.* **1994**, *40*, 111–142.

(50) Casal, H. L.; Mantsch, H. H. *Biochim. Biophys. Acta* **1984**, *779*, 381.
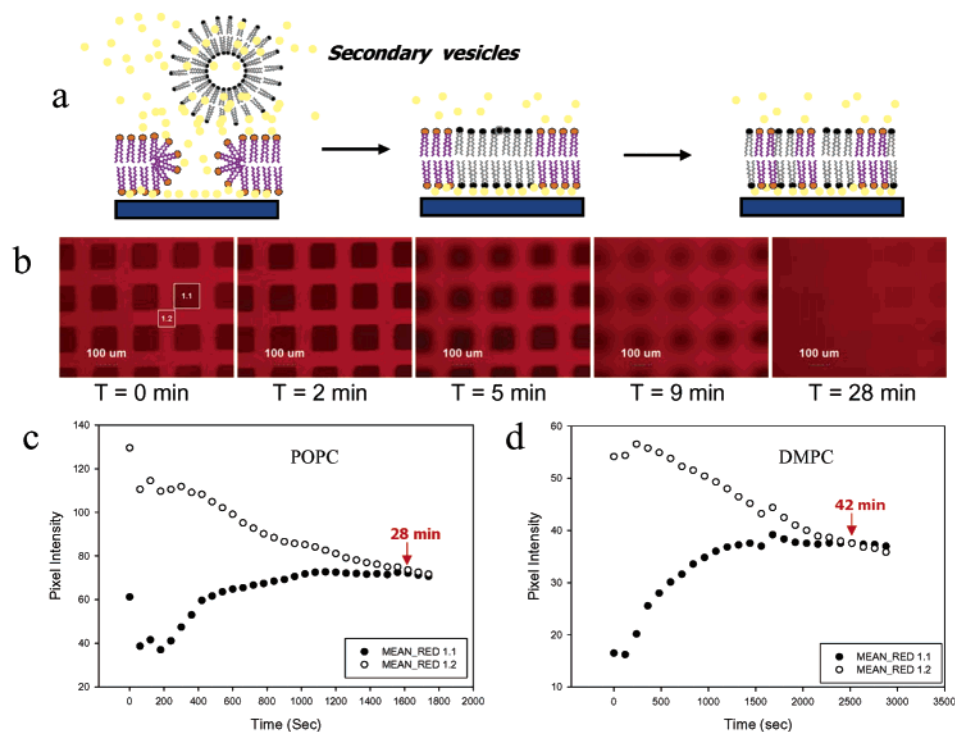
Figure 5. Secondary backfilling of lipid vesicles in void patterns. (a) A schematic representation of the proposed backfilling process. (b) Selected frames from time-lapse epifluorescence images revealing targeted vesicle spreading and pattern erasure upon secondary incubation of unlabeled POPC vesicles within the void regions of a UV-patterned POPC bilayer doped wioth TR-DHPE. (c, d) Fluorescence homogenization curves for two distinctly different regions of interest, 1.1 and 1.2, of the square pattern upon secondary incubations with (c) POPC and (d) DMPC vesicles.

these absorptions including the exact location of the peaks, their full widths at half-maximum, and their relative intensity distributions are in good general agreement with the earlier reports of infrared spectra for the POPC bilayers. The exact locations of the methylene symmetric and antisymmetric stretching, d^+ and d^-, modes are well-known diagnostic markers in the determination of chain-conformational order. In solid crystalline phases, the symmetric methylene stretches (d^+) of alkyl chains absorb between 2848 and 2850 cm^{-1}, and the antisymmetric stretches (d^-) occur between 2916 and 2918 cm^{-1}. For a conformationally disordered liquid phase, however, absorptions due to d^+ and d^- modes occur at distinctly higher ranges of 2856−2858 and 2924−2928 cm^{-1}, respectively.[51] The observed frequencies of 2852 and 2923 cm^{-1} for POPC bilayers suggest that the bilayer assembly is made of partially ordered chains consistent with the expectation for molecules above their transition temperature. In the spectrum for the UV-illuminated samples, no such absorptions are observed above the noise level, indicating the absence of acyl chains or other organic debris after the photooxidation process. A detailed spectral analysis in conjunction with in situ and spatially resolved FTIR microscopy measurements will be separately reported.

Compositional Manipulations by Void Backfilling. An attractive feature of the patterning method developed here is that the voids can be backfilled by subsequent exposures to the same or a different vesicular solution. This way it is possible to manipulate membrane compositions and dynamically probe lipid−lipid diffusive processes. To explore this possibility, we exposed the POPC bilayer samples patterned using the photochemical method above to small unilamellar vesicles of the same lipids. To allow discrimination between the secondary back-

filling phase and the primary patterned bilayer, the incoming vesicles were unlabeled. The initial patterned bilayer was doped with 1 mol % TR-DHPE. The time-lapse images shown in Figure 5b reveal that, upon incubation, the initial nonfluorescent voids began to acquire fluorescence from the background. The images reveal that in all cases the initial pattern was gradually erased, which in approximately 28 min led to the complete homogenization of the fluorophore intensity across the entire POPC surface, eliminating the pattern. A closer examination of the pattern erasures revealed that in all cases the initial square pattern shapes led to an intermediate circular shape, consistent with random Brownian motion of the labeled lipids,[52] before complete erasure was observed. When the secondary incoming vesicles were doped with NBD-DHPE (emission in green), we observed the gradual spreading of both red (TR-DHPE) and green (NBD-DHPE).

Several features of the backfilling experiments are noteworthy. First, the ability to erase the patterns establishes that the void barriers are accessible for further deposition of bilayer-compatible molecules. This observation is further consistent with the scenario deduced from infrared spectra that the void barriers do not contain any lipidic residues but expose the underlying substrate surface via the PBS interface. This is in sharp contrast to many previously developed patterning methods where the barrier materials offer permanent resistance to vesicle fusion. Second, the use of NBD-labeled vesicles during the backfilling stage revealed unambiguously that the incoming vesicles target the void areas directly and exclusively. Third, the time required for completely erasing the pattern was qualitatively comparable

(51) Synder, R. G.; Schachtsneider, J. H. *Spectrochim. Acta* **1963**, *19*, 85−116.

(52) (a) Lee, G. M.; Ishihara, A.; Jacobson K. *Proc. Natl. Acad. Sci. U.S.A.* **1991**, *88*, 6274−6278. (b) Groves, J. T.; Boxer, S. G.; McConnell, H. M. *J. Phys. Chem. B* **2000**, *104*, 119−124. (c) Axelrod, D.; Wight, A.; Webb, W.; Horwitz, A. *Biochemistry* **1978**, *17*, 3604−3609.

to that required for fluorescence recovery for comparable photobleached spots. This observation suggests that the vesicle incorporation stage must be significantly fast in comparison to fluorophore diffusion. Taken together, we assess that the gradual erasure of the pattern suggests that the incoming secondary vesicles must fuse with the surface at the unoccupied void regions of the pattern, forming a nonfluorescent bilayer, and become contiguous with the existing fluorescent bilayer through bilayer−bilayer fusion at the edges, followed by the rate-determining thermal diffusion of fluorophores. The use of separate fluorophore lipids for the primary patterned bilayer and the secondary intercalating bilayer indicated clearly that the spreading of the secondary bilayer within the voids was immediate (within a few seconds), further suggesting that the rates of pattern erasures or fluorescence homogenizations simply measured the diffusion of the probes across the bilayer medium. In this regard, the experiments provide a useful approach to simultaneously measure the diffusional properties of multiple probes within a single bilayer medium.

To further extend this strategy by introducing secondary lipids and lipid mixtures of significantly different translational mobilities, we used stiffer (high-transition-temperature lipids, e.g., DMPC) phospholipid vesicles as sources of secondary lipids. When incubated with patterned samples of POPC, the DMPC vesicles occupied the lipid-free regions, but took a noticeably longer time (∼42 min in comparison with 28 min for POPC for a $100 \times 100 \ \mu m^2$ void) to "erase" the fluorescently visible pattern of the primary POPC bilayer as seen in Figure 5d. In this way, the chemical composition of the parent bilayer can be systematically altered. When the secondary vesicles contained a lipid mixture believed to facilitate lipid raft formation[53] (e.g., 37% POPC, 30% cholesterol, 28% sphingomyelin, 2% GM1, and 3% NBD-DHPE), no diffusion of labeled species (NBD-DHPE or TR-DHPE) across the patterned features occurred for several hours. Images shown in Figure 6 remained unchanged for several hours. This observation suggests the possibility that lipid microdomains (and their aggregates) can be incorporated at predefined locations within a fluid sBLM background.

Discussion

UV Photolithographic Pattern Transfer. Results presented in this paper establish that membrane photolithography employing short-wavelength UV radiation simply by exposure to a low- or medium-pressure Hg lamp through a physical mask can be used to *directly* pattern fluid phospholipid bilayers on solid supports fully submerged in aqueous ambients. Epifluorescence images confirmed the formation of patterns of fluorescence, whereas companion FTIR evidence established that the UV-illuminated regions become lipid-free. Further support for the latter was obtained in the backfilling experiments. Here, the exposure of patterned bilayers to vesicles of the same lipids filled the lipid-free voids, establishing contiguity with the existing membrane patches. When UV-transparent features in the mask are discrete, a pattern of holes is produced, and conversely, with the use of masks displaying islands of UV-opaque features, corralled membranes result. The overall shapes, sizes, and distribution of patterns in the mask are replicated within the bilayer with high definition except at the corners that
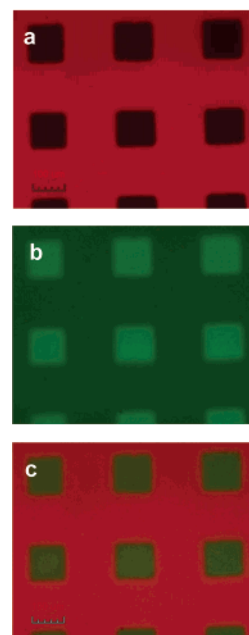

Figure 6. Typical epifluorescence images for patterned TR-DHPE-doped POPC bilayers backfilled with mixed-lipid vesicles containing 37% POPC, 30% cholesterol, 28% sphingomyelin, 2% GM₁, and 3% NBD-DHPE. The images are shown for TR excitation (red), NBD excitation (green), and a two-color overlay using the false-color method. The images remained unchanged for at least 6 h.

appear rounded in epifluorescence images. Microscopy-based imaging fluorescence photobleach recovery measurements on fluid phospholipid bilayers (e.g., DMPC, POPC, and egg-PC mixtures) confirmed that the residual bilayers in the unexposed parts of the pattern retain their long-range fluidity. A semi-quantitative comparison of fluorescent probe diffusional properties in the unpatterned bilayers (before patterning) and un-illuminated regions of the patterned bilayers yielded comparable values (∼2 μm^2/s) even in the vicinity of the holes, suggesting that the formation of a pattern did not measurably perturb the bilayer fluidity.

The approach was found to be independent of the degree of unsaturation in acyl chains, the lipid headgroup chemical structure, the phase state of the bilayer, or the fluorophores used.[54] Moreover, the approach worked equally well when lipid mixtures, including cholesterol and sphingolipids, were used to prepare supported membranes. The generality of our approach was also tested on a wide range of hydrophilic substrates. The use of a coverglass, quartz, mica, and oxided silicon wafers produced comparable results. Further, when hybrid supported bilayers formed by the formation of half-bilayers on alkanethiol-coated Au[55] and long-chain-silane-coated Si substrates[56] were used, the membrane photolithography led to the creation of patterns where UV-illuminated regions displayed removal of the lipid leaflet and the underlying monolayer, exposing the substrate to the ambient buffer (data not shown). Furthermore,

(53) Simons, K.; Ikonen, E. *Science* **2000**, *290*, 1721−1726.

(54) The fluorophores were used only to aid in the imaging of phospholipid bilayers and did not play an active role in UV patterning. Indeed, the UV photolithography process was independent of the type of fluorophore used. Recently, using null-ellipsometric imaging, we have shown the direct photochemical patterning of phospholipid bilayers not stained with any fluorescent probe (M. C. Howland, A. N. Parikh, unpublished data).

(55) (a) Plant, A. L. *Langmuir* **1993**, *9*, 2764−2767. Meuse, C. W.; Krueger, S.; Majkrzak, C. F.; Dura, J. A.; Fu, F.; Connor, J. T.; Plant, A. L. *Biophys. J.* **1998**, *74*, 1388−1398.

(56) Parikh, A. N.; Beers, J. D.; Shreve, A. P.; Swanson, B. I. *Langmuir* **1999**, *15*, 5369−5381.

in all cases, the patterns of holes or of corralled bilayers displayed long-term stability, retaining their geometric shapes, sizes, and distribution as well as their relative position on the substrate surface.

Taken together, we assess that the UV photolithography approach presents an optically defined alternative for directly patterning membranes in aqueous phases by localized photochemical degradation and removal of the exposed lipids, leaving behind fluid films that display optically defined patterns in predetermined geometries. The method does not require any photosensitive molecules or any postexposure development steps. The resulting patterned membranes are comparable to those obtained by the microcontact printing method since both methods expose the underlying substrates at the pattern barriers and allow backfilling. In this vein, the UV-patterned membranes differ from those obtained by deposition of exogenous materials[30] as barriers since the barrier regions in the latter approaches cannot be easily used to erase patterns or engineer molecular heterogeneity such as by backfilling. Moreover, the UV photolithography can be straightforwardly extended to pattern lipid bilayers deposited on curved substrates (e.g., colloids and fibers).

Proposed Mechanism. Two key processes form the mechanistic basis of membrane lithography: (1) spatially confined photochemical degradation of lipid molecules in the UV-exposed areas and (2) stabilization of void regions presumably by hemimicelle formation at the pattern edges.

Low- to medium-pressure Hg lamps used in the present study nominally produce two wavelengths that are relevant to the photodegradation process, 184.9 and 253.7 nm. The shorter wavelength, 184.9 nm, is absorbed by O_2 dissolved in the aqueous buffer, producing ozone and singlet molecular oxygen ($^1O_2^*$), both of which are strong oxidizing agents. The 253.7 nm light is not absorbed by O_2, but by the lipid molecules and also by ozone (O_3). The absorption by O_3 is self-destructive; therefore, under UV light, ozone is continually being formed and destroyed. A byproduct of this reaction cycle is $^1O_2^*$. Finally, the absorption of 253.7 nm light by the organic lipids excites and/or dissociates them, thereby producing activated species, such as ions, free radicals, and excited molecules. These activated molecular and ionic species are then readily attacked by $^1O_2^*$ and O_3 to form smaller molecules, such as CO_2, CO, H_2O, N_2, and other lipid fragments which dissolve readily in PBS. Such photodegradation of organics using short-wavelength UV radiation is well-appreciated in the literature and has long been used in wastewater treatment[57] and in cleaning semiconductor surfaces in air or vacuum.[58] The quantitative interplay between the above photooxidation reactions is significantly more complex. Direct monitoring of the products of the UV-induced lipid degradation using real-time ATR-FTIR spectroscopy is currently in progress in our laboratory.

Next, this photooxidation process exhibits a remarkable lateral confinement presumably due to the short-lived nature of $^1O_2^*$ and O_3, and the requirement of photoexcitation of lipid molecules. Stable patterns form even when the bilayers are "overexposed" to UV light for several hours, suggesting a self-limiting character of the UV photochemistry. This mechanism suggests an interesting parallel with a recently proposed role

of O_3 as a broadly applicable effector molecule in biological immune systems. In a series of studies, Wentworth and co-workers[59] have suggested that the O_3 (and possibly other related oxidants) produced at the site of antibody−antigen union by the antibody-catalyzed water oxidation processes punctures highly localized holes in the bacterial plasma membranes, subsequently killing their antigenic targets.

Spatially directed exposure of sBLMs to short-wavelength UV light, in conjunction with the production of strong oxidants, resulted in the formation of stable microsocopic sBLM patterns by molecular degradation of exposed lipids, leaving behind stable voids or disjointed membrane patches at optically defined locations on a substrate surface. The laterally selective removal of lipid molecules by UV exposure must create an energetically unfavorable interface, exposing hydrophobic lipid chains to the aqueous medium at the boundary (Figure 1a). Relaxation of the associated line tension can occur via large-scale stretching of the remaining bilayer only if a source for additional lipids is available such as through suppression of undulations.[60] Our results suggest that phospholipid bilayers supported on planar solids do not possess such accessible lipids in significant quantities required for healing the large micrometer-scale voids created. We further observe that the void regions are stable for long periods of time, consistent with the notion that such large-scale density reductions require unfavorable energy penalties associated with the reduction in van der Waals forces between the lipid chains. It appears reasonable that the borders shield the hydrophobic lipidic chains from the aqueous ambient through spontaneous structural reorganization of the lipids presumably into a closed hemimicellar microphase. Indeed, several theoretical studies invoking the use of membrane elasticity theory have recently appeared in the literature that predict that the edges of the lipid bilayer fronts (such as formed during vesicle spreading at surfaces) and walls of the membrane pores organize into a hemimicellar structure.[61−64]

An intriguing aspect of the results presented here is that the voids retain arbitrary geometric shapes and sizes (micrometer scale and above) within fluid bilayer media. It is tempting to expect that the void perimeters will relax into pseudo-two-dimensional circular morphologies to minimize the line tension. Such large-scale circularization of the micrometer-scale void shapes was not observed for several void shapes including triangular, stripe, and rectangular. In all cases, however, sharp corners appeared rounded in the epifluorescence images of the bilayer pattern.

To further examine if the stability of the void shapes is an artifact of the local photochemical processes, we prepared similar patterns by microcontact printing, which does not involve any photochemical modifications. Fluorescence patterns of square-shaped voids (data not shown) produced by the latter technique also revealed the stabilization of noncircular voids. Furthermore, these observations are consistent with isolated membrane patches in square geometries reported previously by

(57) Legrini, O.; Oliveros, E.; Braun, A. M. *Chem. Rev.* **1993**, *93*, 671−698.
(58) Vig, J. R. *J. Vac. Sci. Technol., A* **1985**, *3*, 1027−1034.

(59) (a) Wentworth, P.; et al. *Science* **2002**, *298*, 2195−2199. (b) Wentworth, P.; et al. *Science* **2001**, *293*, 1806−1811.
(60) Sandre, O.; Moreaux, L.; Brochard-Wyart, F. *Proc. Natl. Acad. Sci. U.S.A.* **1999**, *96*, 10591−10596.
(61) Nissen, J.; Gritsch, S.; Wiegand, G.; Radler, J. O. *Eur. Phy. J. B* **1999**, *10*, 335−344.
(62) Fosnaric, M.; Kralj-Iglic, V.; Bohinc, K.; Iglic, A.; May, S. *J. Phys. Chem. B* **2003**, *107*, 12519−12526.
(63) May, S. *Eur. Phy. J. E* **2000**, *3*, 37−44.
(64) Betterton, M. D.; Brenner, M. P. *Phys. Rev. Lett.* **1999**, *82*, 1598−1601.

Hovis and Boxer[38,39,65] These comparisons suggest that the formation of stable voids in arbitrary shapes within fluid phospholipid bilayers does not result from photochemical treatment but may result from other patterning methods. Next, our preliminary thermal study also revealed that the patterns can be erased by annealing the patterned samples at elevated (65 °C) temperatures. On the basis of the above, it appears that the edge stablization is a more complex problem presumably influenced by membrane elasticity, fluidity, and a competition of electrostatic and van der Waals interactions as has been previously suggested.[63]

We could not directly assess if the unexposed parts of the bilayer were contaminated by any bilayer-compatible or other partially oxidized products such as may be produced during the UV photooxidation and diffused into the fluid, unperturbed membrane patches. However, several lines of evidence point to the minimal presence of any such partially photodamaged lipids within the remaining lipids or at the edges. First, the analysis of FRAP data suggests that the membrane fluidity remains essentially unchanged upon patterning and the fraction of "immobile" lipids remains below our measurement capability. Second, the FTIR spectroscopy data do not show any new vibrational absorption modes such as can be expected for any oxidized lipid. Third, note the ability of the new vesicles to access the membrane voids and become contiguous with the existing residual membranes, thereby erasing the patterns. The time required for complete pattern erasure or Texas Red fluorescence homogenization (∼28 min) when an unlabeled POPC bilayer phase was introduced within the voids (Figure 5) of the patterned POPC bilayer doped with TR-DHPE compares well with that expected on the basis of thermal mixing alone and does not appear hindered. These three independent pieces of evidence strongly suggest that the contaminants, if any, do not perturb the biophysical properties of the residual membrane. These observations further support our earlier conclusion that no significant organic debris is present at the pattern edges or in the interior of the lipid-free void features.

Backfilling Patterned Membranes as a Means To Study Lateral Dynamics in Bilayer Media. Pattern erasure and compositional manipulation data (Figures 5 and 6) illustrate the usefulness of the photochemical patterning approach in manipulating membrane compositions, studying the dynamics of lipid–lipid mixing, phase separation, and metastability, and engineering long-lived (kinetically trapped) functional microdomains or heterogeneities within an otherwise homogeneous lipid bilayer. The approach makes it possible to juxtapose a distinct lipidic environment separated by aribitrary, well-defined diffusive interfaces by simply backfilling primary patterned bilayers using vesicles of different lipids and their mixtures. Subsequent evolution of the patterns via mixing can be used to study lipid–lipid interdiffusion and probe partitioning preferences and potentially reactive–diffusive processes within membrane media. In this regard, the approach offers a powerful tool to understand the phase stability and dynamics of multicomponent lipid bilayers, potentially providing useful insights into how complex cellular membranes handle their heterogene-

ity. Further, as illustrated by the experiment involving backfilling by cholesterol and sphingomyelin mixtures, the approach can be used to kinetically arrest the mixing of different lipidic components into long-lived artificial patterns, thereby allowing a means to engineer membrane heterogeneities at predefined locations within synthetic bilayer media (Figure 6). The observed isolation of the raft-forming mixed bilayer from the POPC primary phase can be understood in terms of kinetic frustration in mixing. It is now well-established that raft-forming lipid mixtures phase separate in cholesterol-rich microdomains from a lipid-enriched background.[66] Thus, the patterns observed in Figure 5 may represent three coexisting phases: The green squares comprise a liquid-ordered raftlike phase rich in cholesterol and sphingomyelin surrounded by a liquid-disordered phase enriched in the phospholipid POPC. The red background represents the third POPC phase. It is further believed that NBD-DHPE shows a preference for liquid-ordered phases in lipid bilayers.[66,67] That no diffusion of NBD-DHPE was seen across the patterned features is consistent with low mobilities of raftlike domains (within which NBD-DHPE preferentially resides) that remain kinetically trapped within the initial square domains. When the cholesterol concentration in the secondary phase was lowered to below 20 mol %, gradual fluorophore mixing was observed. A systematic account of these observations will be separately reported.

Conclusions

In summary, the wet membrane photolithography approach presented here is simple and inexpensive and is an enabling procedure to create optically defined patterns of fluid bilayer lipid membranes submerged in the aqueous phase. The void "barriers" separating the lipid bilayers by this technique are accessible for secondary intercalation with distinct lipids whose approach to equilibrium via diffusive mixing can be monitored, and the physical basis of the material heterogeneity of membranes can be studied. Moreover, spatially directed insertion of functional substructures (e.g., receptors, antibodies, and proteins) is possible. Furthermore, the process itself, involving spatially confined production and use of potent oxidants, may be useful for model studies of oxidative stress to cells and in examining their role in immune systems. Taken together, the approach provides a useful platform for the study of many membrane processes. The membrane lithography involving spatially directed photodegradation of bilayer lipids using patterned UV illumination extends in the aqueous phase the widely popular methods of light-directed syntheses for designing peptides or DNA sequences on planar supports in the dry state. The ability to backfill the void barriers further provides a new means for manipulating membrane composition and studying a wide class of reactive–diffusive membrane processes (e.g., lipid–lipid phase behavior and probe partitioning) by providing artificially designed diffusive interfaces where distinct bilayer lipid phases can be juxtaposed and their dynamics probed. In conjunction with multiple patterning and backfilling cycles, the approach may also open up interesting possibilities for synthesizing optically defined microarrays of functional membrane substructures, protein-binding sites, and membrane proteins.

(65) Hovis and Boxer (ref 38) suggested that the formation of stable hydrophilic voids separating the membrane fluid can be understood in terms of material deficiency. Once sufficient lipid material has been removed during the patterning process, the remaining lipid phase may undergo slight edge expansion and rounding-off at pattern edges. No large-scale circularization of pattern features was observed in that study.

(66) Dietrich, C.; Bagatolli, L. A.; Volovyk, Z. N.; Thompson, N. L.; Levi, M.; Jacobson K.; Gratton, E. *Biophys. J.* **2001**, *80*, 1417–1428.
(67) Klausner, R. D.; Wolf, D. E. *Biochemistry* **1980**, *19*, 6199–6203.

JA047714K